Journal of Molecular Catalysis A: Chemical 308 (2009) 87–95

Contents lists available at ScienceDirect

Journal of Molecular Catalysis A: Chemical

journal homepage: www.elsevier.com/locate/molcata

Silica supported Pt/Ni alloys prepared via co-precipitation method

N.H.H. Abu Bakar[a,b], M.M. Bettahar[a,*], M. Abu Bakar[b], S. Monteverdi[a], J. Ismail[b], M. Alnot[c]

[a] UMR CNRS-UHP 7565, ICPCJB, Faculté des Sciences, Université Henri Poincare, Nancy 1, BP 239, 54506 Vandoeuvre Cedex, France
[b] School of Chemical Sciences, Universiti Sains Malaysia, 11800 Gelugor, P.Pinang, Malaysia
[c] Laboratoire de Physique des Matériaux, UMR 7556, Université Henri Poincare, Nancy 1, BP 239, 54506 Vandoeuvre Cedex, France

ARTICLE INFO

Article history:
Received 25 November 2008
Accepted 22 March 2009
Available online 31 March 2009

Keywords:
Pt/Ni nanoparticles
Silica support
Co-precipitation
Hydrogenation activity

ABSTRACT

Pt/Ni alloyed nanoparticles have been prepared via co-precipitation method on crystalline silica support. The respective salt solutions were reduced using sodium borohydride ($NaBH_4$) in an inert atmosphere at 353 K. Various Pt/Ni molar ratios were studied. H_2-TPR studies revealed that total reduction of the metal ions occurred during the reduction stage while H_2-TPD profiles show that there are four different types of the catalysts. Catalytic studies of these bimetallic catalysts demonstrate enhancements in the activity compared to Ni_{100}. Catalyst with the best activity, $Pt_{72}Ni_{28}$, exhibits specific metal sites not seen in other catalysts. The existence of these metal sites is explained as due to the interaction between Pt and Ni nanoparticles. STEM analysis strongly indicates that the nature of the interaction is the formation of alloys between the metal particles while XPS demonstrates that Pt segregation occurs on the surface of the bimetallic particles.

1. Introduction

Supported metal nanocatalysts have been given great attention for many years. They play significant roles in various industries such as in portable electronic products, production of nylons [1] and most importantly in fuel cells [2,3]. With the rapid development of technology, the demand for such active materials has increased considerably. This has led to numerous studies among others on the synthesizing and characterization of better efficiency catalysts. Various metals, supports and synthesis conditions have been investigated. This has inadvertently brought about the increasing interest in supported alloys as one of the main studied catalyst materials. Nevertheless, these catalyst materials still lack comprehensive fundamental understanding. For this reason, much work has been focused on studying not only the properties of these materials but also their synthesis conditions.

Traditionally, supported alloys are usually synthesized using two or more metal precursors/metals at extreme temperatures. This technique is well known and has been reported comprehensively [4–6]. This classical approach is recognized for its simplicity and clean resultant alloyed material, nevertheless it has several disadvantages. One of the major drawbacks of this method is the increase in particle size with increasing temperature and heating periods [7]. These treatments are employed to ensure the formation of crystalline alloys as well as for drying and activation purposes. This phenomenon has been described in several systems such as for alloy electrocatalysts [4], $Pt_{70}Co_{30}$ and the Pt/Ru supported on carbon [5]. It is this shortcoming that eventually led to the development of other methods of alloying in the catalyst preparations.

Generally, chemical reduction, electroplating as well as mechanical milling [8] are some of the alternative (non-classical) alloying techniques employed. Chemical reduction methods use reducing agents such as borohydrides [9–13], hydrazine [14–16], formaldehyde [17–18] and alcohols [18–20]. This chemical reduction method has been reported to produce both dispersed and small sized particles at low temperatures. The main reason for such favorable features is the enhanced reduction rate of the precursors [15]. Even so, it is noted that although this method is capable of efficiently synthesizing the bimetallic nanoparticles, it does not guarantee the formation of crystalline alloys and the particle is still prone to oxidation. Hence, many researchers have employed thermal treatments at high temperatures for long durations even after reduction of the metal salts [11,16,21]. This method was employed by Mattei [22] who reported the synthesis of non-alloyed bimetallic particles with core-shell morphology while other researches [15,23] demonstrated the formation of alloyed bimetallic nanoparticles with similar morphology. Though this non-classical method may prove to enhance catalytic activity via the formation of smaller particles when compared to the classical methods, the thermal treatments used may hinder the actual potential of the catalyst due to the increase in particle size during alloy formation as previously mentioned. Therefore understanding the factors that govern the alloy formation and their manipulation is significant.

* Corresponding author. Tel.: +33 83 68 49 48; fax: +33 83 68 49 55.
E-mail address: mohammed.bettahar@lcah.uhp-nancy.fr (M.M. Bettahar).

1381-1169/$ – see front matter © 2009 Elsevier B.V. All rights reserved.
doi:10.1016/j.molcata.2009.03.029

Several aspects can influence the formation of supported alloys. Among them are the miscibility of the metal components, the chemical interaction that occurs with the host matrix and the reduction technique or reducing agent that ultimately influences the nucleation and growth of the nanoparticles [22]. Researches have also observed that other synthesis conditions can be manipulated to induce or enhance alloying of elements. In a recent paper by Antolini and coworkers [10], the effect of reduction temperature as well as $NaBH_4$ concentration on the extent of alloying was reported. Their investigations showed that for Pt/Co nanoparticles, a higher degree of alloying was observed when the metal salts were reduced at temperatures ranging from 0 to 40 °C and with lower concentrations of $NaBH_4$. Similar reaction temperatures have also been used to synthesize Ni/Pd and Ni/Pt alloys employing hydrazine as the reducing agent [14].

Our previous work has revealed that size and shape of supported nickel prepared by a chemical method depended on the reduction conditions [16], the nature of the support [24] and presence of a metal additive [25]. By using hydrazine as the reducing agent, it is found that crystalline silica promoted the reduction of nickel while amorphous silica inhibits the nickel reduction by giving rise Ni ion-silica surface species [24]. In a similar chemical reduction method [25], whereby the bimetallic system is silver (Ag) and Ni, the presence of Ag sharply increased the catalytic activity of Ni. Although silver is known as an inactive catalyst it was found that in the presence of silver, Ni/Ag core-shell groupings are formed which led to an increase in metallic surface area of nickel and consequently to a sharp increase in catalytic activity.

In this work, it is our objective to understand the surface characteristics of the catalysts and describe how it affects the catalytic activity of the supported bimetallic nanoparticles. We, hereby, report the synthesis of Pt/Ni nanoparticles on crystalline silica using sodium borohydride as a reducing agent. The formation of NiB and PtB also considered as metal–metalloid alloys have been reported to promote hydrogenation activities [26]. Catalysts were prepared via co-precipitation technique. The nature of the as prepared catalysts was characterized by transmission electron microscopy (TEM), scanning tunneling electron microscopy (STEM), selected area electron diffraction (SAED) and X-ray photoelectron spectroscopy (XPS). Surface characteristics of the samples were investigated using dynamic flow methods such as H_2 temperature programmed desorption (H_2-TPD) and H_2 temperature programmed reduction (H_2-TPR) analysis. The catalytic activity of the prepared catalysts is evaluated via the hydrogenation of benzene to cyclohexane.

2. Experimental

2.1. Materials

All materials were used without further treatment. Crystalline silica (99.99%) was obtained from Chempur. Platinic chloride ($H_2PtCl_6{\cdot}H_2O$) was purchased from Sigma, nickel (II) sulphate ($NiSO_4{\cdot}6H_2O$) from R & M Chemicals and sodium borohydride ($NaBH_4$) from Riedel de Haen.

2.2. Preparation of catalysts

All the catalysts were prepared via co-precipitation technique. An amount of crystalline silica was weighed and suspended in a mixture of 30 ml of distilled water and 8 ml of ethanol. The suspension was purged with argon at 353 K. Subsequently, various amounts of Pt (0.05 M, 10 ml) and Ni (0.084 M, 100 ml) salt stock solutions were added to the suspension to obtain various mol/mol ratios of Pt:Ni. The various ratios are Ni_{100}, Pt_8 Ni_{92}, $Pt_{21}Ni_{79}$, $Pt_{72}Ni_{28}$ and Pt_{100} (calculated based on AAS analysis). In all cases, the Ni salt solution was added prior to Pt salt solution. The resultant mixtures were homogenized for a duration of 10 min before the addition of 8 ml of 0.2 M fresh cold $NaBH_4$. The reaction was allowed to continue for an additional 15 min before filtering and washing with distilled water. All catalysts were then dried under vacuum conditions.

2.3. Characterization of catalysts

The TEM, STEM-EDX and SAED of all the samples were obtained using a CM20 Philips transmission electron microscopy operating at 20 kV. Fresh catalysts were redispersed in ethanol and a drop of the solution was placed onto carbon coated copper grids. The XRD spectra were recorded in the 2θ range of 10–100° with a Cu Kα radiation. XPS measurements (for C 1s, Si 2p, O 1s, Ni 2p and Pt 4f) were conducted using an ESCALAB MK II VG with Mg Kα and Al Kα radiations.

H_2-TPR experiments were performed on all of the fresh catalysts. Typically, 50 mg of the catalyst was weighed and placed in a reactor. The catalyst was heated at a constant rate of 5 K min^{-1} from room temperature to 1123 K while purging with a mixture of hydrogen and argon (1000 ppm H_2). The total gas flow rate was previously determined as 90 ml min^{-1}. The resultant effluent gas was analyzed on line using an Agilent G2890A microchromatograph operated at 333 K. In the case of H_2-TPD experiments, 50 mg of the catalyst was placed in the reactor. This was then activated at 473 K in pure hydrogen for the duration of 15 min followed by purging with argon (100 ml min^{-1}) for approximately 45 min and finally cooled to room temperature. H_2-TPD analysis was carried out using similar temperature program and detection as for the TPR analysis described earlier.

2.4. Catalytic activity measurements

A series of experiments were conducted to determine the conditions in which optimum activity is achieved. Catalysts were subjected to various heating rates (2, 5, 10 and 15 K min^{-1}) and subsequent activation at 100 or 200 °C in a flow of 100 ml min^{-1} of pure hydrogen. The condition in which optimum activity is obtained was then used to activate the catalysts as described below.

Typically as much as 50 mg of the samples were weighed and placed in a U-shaped reactor. The catalysts were then activated in a flow of 100 ml min^{-1} of pure H_2. Samples were heated to 473 K at a heating rate of 10 K min^{-1}. Upon reaching 473 K, the samples were maintained at the same temperature for another 15 min. Catalysts were then cooled to room temperature and the catalytic activity measurements were conducted by contacting the catalysts with a reaction mixture of 10/40/150 ml min^{-1} benzene/hydrogen/helium. The extent of dilution of the reaction mixture with helium was previously chosen to enable comparison of catalytic activity of the prepared catalysts. The reaction products were fed into a 5730A Hewlett–Packard gas chromatography equipped with a flame ionization detector and 8 m molecular sieve column. Various other temperatures were studied to evaluate the catalytic activity.

2.5. Determination of fractal dimension

The particle's dispersion onto and within the crystalline silica support is evaluated using the fractal technique. Fractal dimensions, D_F, of the samples were determined based on the method described by Liang [27]. This approach involves choosing several centre points in a TEM image of a sample and drawing circles with a radius of r_1, r_2, r_3, …, r_i. Following this, the micrograph is manually digitized using ones and blanks to indicate the presence and absence of par-

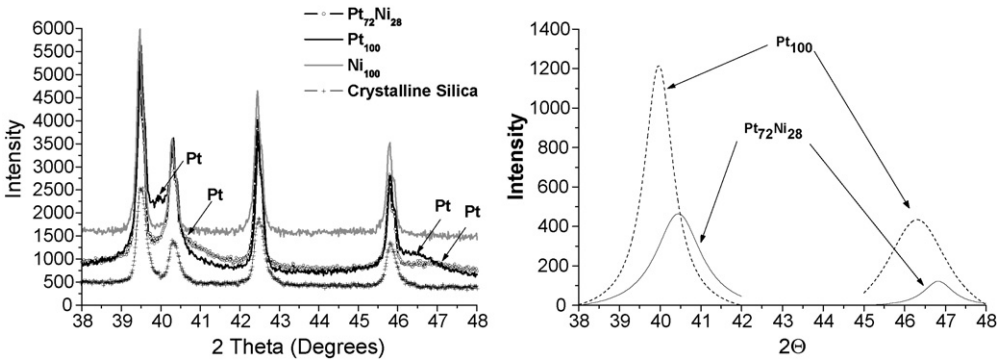

Fig. 1. XRD diffractograms of crystalline silica and fresh catalysts and the respective Pt peaks deconvolution.

ticles. The number of ones (M_i) within a circle of a certain radius is calculated and an average is obtained. Subsequently, by plotting $\ln M$ vs $\ln r$, the D_F value is obtained from the slope of the plot.

2.6. Determination of metal dispersion

Metal dispersion in the catalysts was determined using the mathematical approach proposed by Borodzinski and Bonarowska [28]. The mathematical expressions developed relate the average particle size and their dispersions. For metal particles where $d_i > 24d_{at}$ (where '*at*' is atomic) the dispersion (D_M) is $5.01d_{at} \sum n_i d_i^2 / \sum n_i d_i^3$ while for metal particles with an average particle size of $d_i \leq 24.0d'_{at}$, $D_M = 2.64/d_{rel(VS)}{}^{0.81}$ where $d_{rel(VS)}$ is the relative volume surface mean diameter.

3. Results and discussion

3.1. Structural studies

The XRD analysis of the crystalline silica exhibits peaks at 2θ values of approximately 39.5°, 40.3°, 42.4° and 45.7° as shown in Figs. 1 and 2 for the fresh and activated catalysts respectively. The main peaks for Pt are also positioned at around similar values (39.8 and 46.3) and hence make the determination of the metallic phase of Pt in the samples difficult. The metal particle size which may be small and the low metal content with respect to the silica may have also contributed to the inability to determine the existence of these peaks. Interestingly, the Pt peaks are a little more prominent, after catalyst activation, in both the Pt_{100} and $Pt_{72}Ni_{28}$ catalysts. Deconvolutions of these peaks indicate that a slight shift of the Pt peaks occurs in the $Pt_{72}Ni_{28}$ catalysts when compared to that of Pt_{100}. The Ni_{100}, on the other hand, exhibits no peaks that indicate the formation of Ni or NiO. The unavailability of Ni and NiO peaks is quite surprising considering the nature of Ni which easily agglomerates hence should give rise to strong signals. Even so, this phenomenon may be due to the arrangement of the Ni atoms that forms amorphous Ni or NiO. Similar occurrences have been reported elsewhere for Ni [29]. The Pt peaks shift can be correlated to lattice distortions which arise as a result of the variation in the atomic size of the elements involved. This may lead to the occurrence of surface segregation or to the formation of alloys. Several researches have also attributed the occurrence of surface segregation in PtNi alloys to lattice distortion [30–32] while others indicated the peak shift owing to alloying between Pt and Ni [33,34]. In the latter, Ni atoms are incorporated into the fcc structure of Pt. Similar observations have been reported for the formation of Pt/Co alloys using $NaBH_4$ as a reducing agent at temperatures below 373 K [10].

TEM images of the Ni_{100}, Pt_{100} and $Pt_{72}Ni_{28}$ are shown in the respective Fig. 3(a), (b) and (c). It is observed that in all samples most of the particle formation did not occur on the support but instead the particles occurred surrounding the crystalline silica forming fractal structures. This occurrence can be attributed to the low surface area of the support which limits incorporation of the metal salts along with its solvation in the aqueous phase during the reduction stage. Li et al. also reported possible Ni leaching during reduction with KBH_4 in aqueous solutions, for catalysts calcined at low temperatures prior to the chemical reduction [26]. This is due to the poor interaction between the Ni species and the support which may also have caused the fractal formation surrounding silica in this case. Formation of such morphologies is due to non-equilibrium growth of the particles [35]. This implies that the structure grows in different directions at different rates. Such morphologies have been reported to exhibit unique properties that differ from their

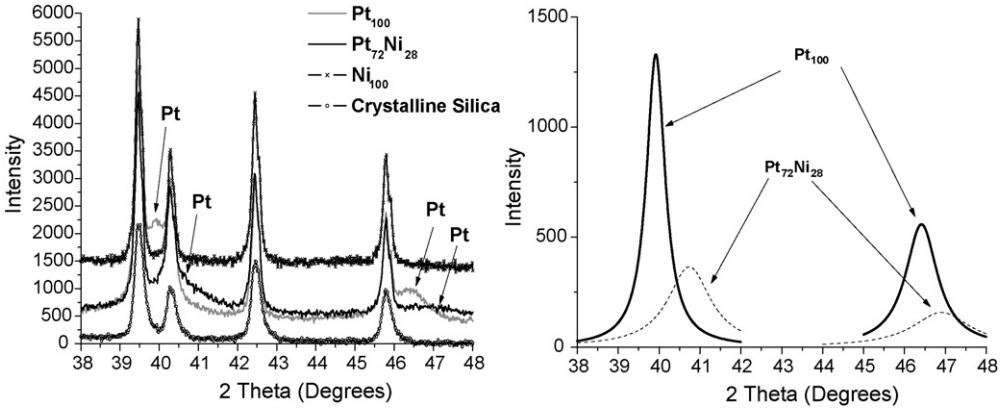

Fig. 2. XRD diffractograms of crystalline silica, activated catalysts and the respective Pt peaks deconvolution.

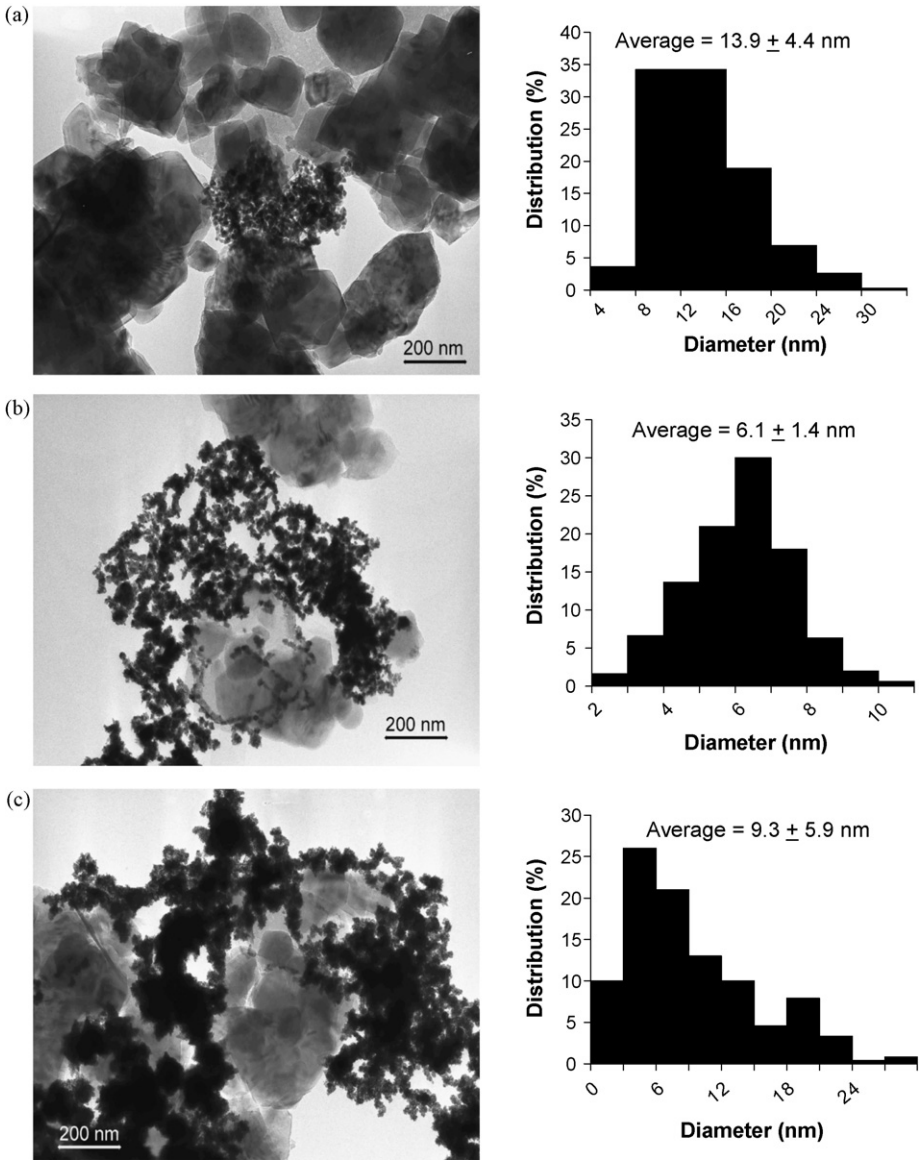

Fig. 3. TEM images and particle size histograms of (a) Ni_{100}, (b) Pt_{100} and (c) $Pt_{72}Ni_{28}$ catalysts supported on crystalline silica.

bulk or isolated particles [36]. These fractal structures have a fractal dimension (D_F) of 2.46, 1.85 and 1.97 for the Ni_{100}, Pt_{100} and $Pt_{72}Ni_{28}$ respectively. According to the previous studies, fractals with different D_F values indicate the nature in which the fractals exist. In general, those with a value of 2 refer to the formation of smooth surfaces while fractals with a D value of more than 2 and less than 2, indicate that rough continuous surfaces and surfaces which are chemically active exist respectively [37]. Based on the D_F values, the Ni_{100} fractals exist as corrugated continuous surfaces. This means that the metal phase is present as large structures of an uneven surface. The type of irregularities in the metal structure can be in the form of humps, cracks, whiskers or even pores [38]. On the other hand, according to Pajkossy and Nyikos [38] both the Pt_{100} and $Pt_{72}Ni_{28}$ samples exhibit fractal dimensions that usually

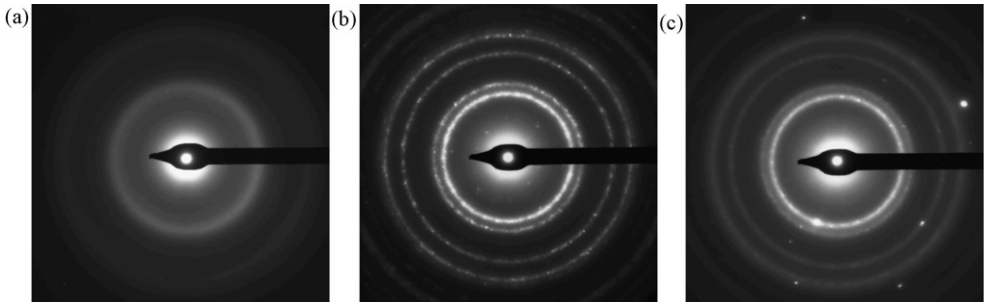

Fig. 4. Electron diffraction of (a) Ni_{100}, (b) Pt_{100} and (c) $Pt_{72}Ni_{28}$ catalysts.

correspond to that of catalysts. They reported that two types of fractals with D_F values less than 2 can occur. Typically, continuous fractals usually have partially blocked active surfaces while non-continuous fractals are described as chemically active islands on inactive supports. In this present work, the fractal growth did not occur on the crystalline silica support and that the fractals formed are that of partially blocked active surfaces. This phenomenon is described to occur, due to the growth of the fractals that occurs in several dimensions hence may cover some of the active sites available. In contrast, the non-continuous fractals are stabilized by the inactive support that inhibits extensive growth and this enables a maximum exposure of the active sites.

Images of the catalysts at higher magnification (not shown here) show that the fractals are composed of small spherical particles. The average particle size of the nanoparticles is 6.1 ± 1.4, 14.0 ± 4.4 and 9.3 ± 5.9 nm for Pt_{100}, Ni_{100} and $Pt_{72}Ni_{28}$ respectively. The size distribution histograms indicate that the Pt_{100} exhibited a narrow size distribution while both Ni_{100} and $Pt_{72}Ni_{28}$ demonstrated particles with a wide size distribution. The reduction in particle size with increasing Pt content may be explained as due to the decrease in the total number of atoms available in the catalysts during the reduction and growth process. The similar total metal content in terms of weight and the higher atomic weight of Pt decreases the number of atoms that can be adsorbed and grow on nucleated metal particles. This results in the smaller particle size. However, the presence of B to a certain extent may also play a role in the reduction of the average particle size as reported previously [39,40]. Dispersion values of the metal phase [28] in the catalysts are 46.6%, 9.9% and 36.8% for the Pt_{100}, Ni_{100} and $Pt_{72}Ni_{28}$ samples respectively. Comparison of the metal dispersity of these samples with other works [34,41] showed that similar values were obtained, although different determination methods were used.

The electron diffraction patterns are shown in Fig. 4. The pattern of Ni_{100} as in Fig. 4(a) is seen to be very diffuse and have less intense rings. Hence this correlates with the XRD results that indeed amorphous Ni occurs in the catalyst. Samples of Pt_{100} and $Pt_{72}Ni_{28}$, on the other hand, exhibit finer rings that are more intense, owing to the polycrystalline nature of the metal particles. Based on these patterns, the d spacings for the Pt_{100} is 2.33, 1.96, 1.40 and 1.19 Å. These values are attributed to the (1 1 1), (2 0 0), (2 2 0) and (3 1 1) planes of the fcc structure of Pt [42]. For $Pt_{72}Ni_{28}$, the d spacings are 2.27, 1.96, 1.38 and 1.16 Å. These values are similar to that of Pt_{100}. No additional rings assigned to Ni exists, hence indicates that alloying occurs in the $Pt_{72}Ni_{28}$ sample whereby Ni is incorporated into the Pt fcc lattice.

The line profiles of the $Pt_{72}Ni_{28}$, as shown in Fig. 5, also confirmed that most of the metal particles are not incorporated into the crystalline silica support. The profiles of Si and O are similar and thus indicate that only silica and no other metal or oxides exists in the samples. The profiles of both the Pt and Ni metals are almost identically matched. Hence, this further elucidates the formation of Pt/Ni alloys in the $Pt_{72}Ni_{28}$ catalyst. This reaffirms the result obtained from the SAED analysis previously described.

3.2. Surface characteristics

3.2.1. H_2-TPR

It is expected that all metal particles are in the reduced state following the reduction of the metal ions in inert conditions. However, possible superficial oxidation of the metal phase may have occurred as a result of storing the catalysts in atmospheric conditions. H_2-TPR analysis was conducted to investigate the state of the metallic phase in the fresh catalysts. Fig. 6 illustrates the H_2-TPR profiles obtained. It is obvious that for all catalysts, the consumption of H_2 does not occur in the temperature range studied. No consumption peaks are observed for Ni oxides although nickel is known to easily

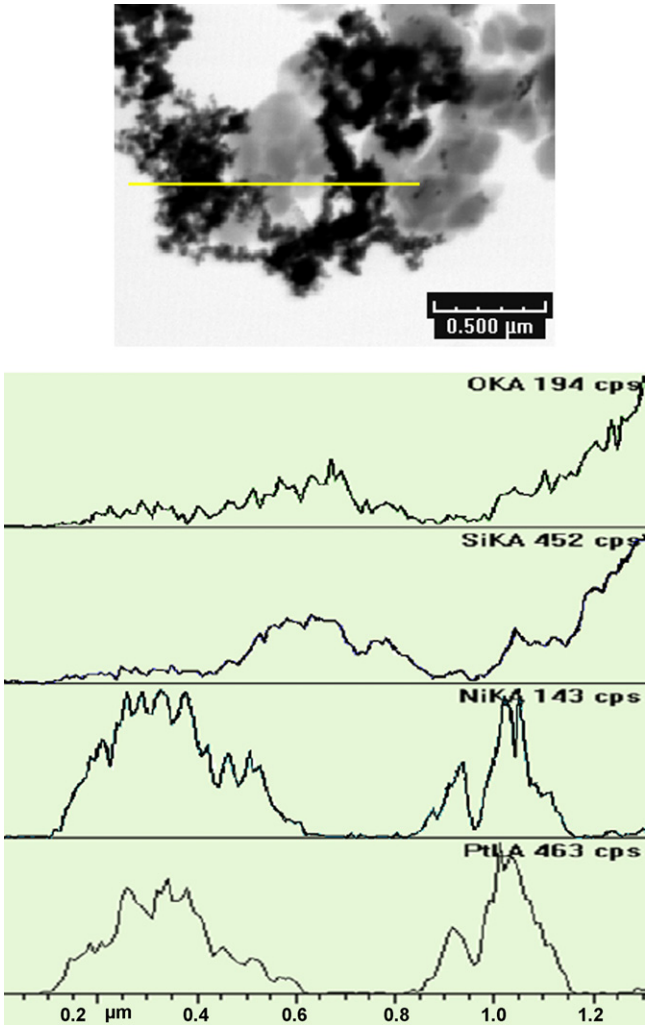

Fig. 5. Line profiles of $Pt_{72}Ni_{28}$ supported on crystalline silica.

oxidize due to its high negative potential. This is indicative of the occurrence of total reduction of the metal ions during the preparation stage and the catalysts are stable towards oxidation even when exposed to air during storage of the samples. This is similarly observed by Li et al. [9] who studied the formation of Pt/Ni supported on carbon. However, in their work, they observed the

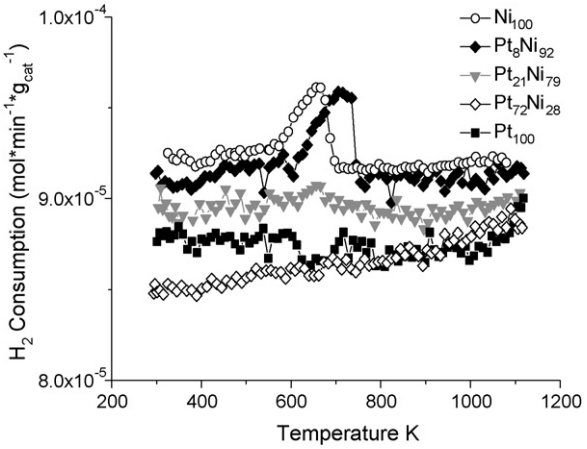

Fig. 6. H_2-TPR profiles of the various fresh Pt/Ni catalysts supported on crystalline silica.

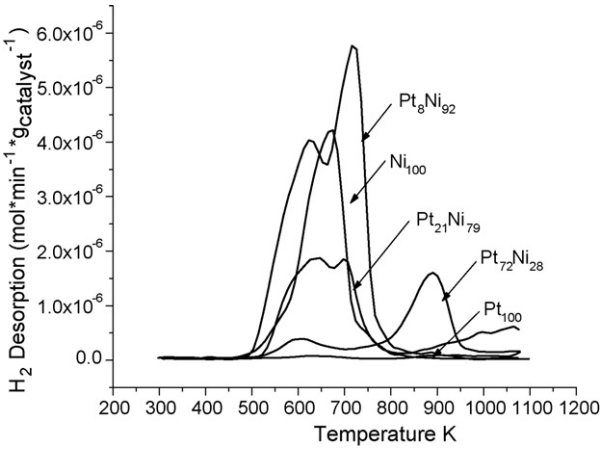

Fig. 7. H_2-TPD profiles of the various Pt/Ni catalysts supported on crystalline silica.

consumption peaks positioned at 243–303 K that are attributed to the formation of PtO. In the present work, such peaks would not have been observed due to the limited temperature range studied.

The profiles of Fig. 6 indicate that the production of hydrogen occurs for samples with high Ni content (i.e. Ni_{100} and Pt_8Ni_{92}). The production of the hydrogen occurs in the temperature range of 600–760 K and is attributed to H_2 strongly adsorbed onto the metallic surface. As much as 4.1×10^{-3} and 4.8×10^{-3} mol $g_{met}{}^{-1}$ H_2 were produced by Ni_{100} and Pt_8Ni_{92} catalysts respectively. This desorption may be explained as due to several factors; the excess of borohydride ions not removed from the catalysts after washing, adsorption of hydrogen gas during the preparation stage or adsorption of hydrogen during the TPR experiment at low temperature. To determine the contributing factor, a sample containing only silica and $NaBH_4$ was similarly analyzed using H_2-TPR. The results showed that no desorption of hydrogen occurred from both materials. Hence it can be summarized that the production of hydrogen from high Ni content catalyst samples is possibly due to the adsorption of the gas molecules during the reaction of metal ions with $NaBH_4$ or at low temperatures during TPR experiment.

3.2.2. H_2-TPD analysis

Fig. 7 exhibits the H_2-TPD profiles. These profiles suggest that there exist four distinct types of catalysts, that of Ni_{100}, those with high amounts of Ni content (Pt_8Ni_{92} and $Pt_{21}Ni_{79}$), Pt_{100} and that with high Pt content ($Pt_{72}Ni_{28}$). The first type of catalyst, Ni_{100}, desorbs hydrogen at approximately 500–800 K with a maximum at 670 K. The second type of catalyst also desorbed hydrogen in a similar temperature range but the incorporation of Pt resulted in the formation of additional adsorption sites. Deconvolution of peaks of these two types of catalyst demonstrates that both catalysts are comprised of four peaks positioned at approximately 570–610, 625–640, 690–705 and 700–745 K. Inspection showed that, upon addition of Pt, the Ni peak is shifted from 670 K to lower temperatures range of 625–640 K. Another interesting observation is that the peaks attributed to the Ni_{100} as well as that of Pt_8Ni_{92} and $Pt_{21}Ni_{79}$ catalysts (at 625–745 K) roughly coincide with those of the H_2-TPR profiles of Fig. 6. Previous works have shown that these peaks arise due to several factors: H_2 strongly bonded to the Ni particles, hydrogen retained at the metal support interphase or H_2 incorporated in the support as spilt-over species [43]. Adsorption of H_2 in this case may have occurred during the preparation stage when the metal ions were reduced with $NaBH_4$ or otherwise during the activation step. As for the peaks positioned at lower temperatures, these are explainable as due to H_2 loosely bound to the metal surface. The third type of catalyst, Pt_{100}, exhibits three peaks of different characteristics. The first peak is centred at room temperature and is due to very loosely bound hydrogen atom from dissociated hydrogen molecule. The second peak is positioned at 638 K and is similar to that observed in the second type of catalyst (high to moderate amounts of Ni content) and is ascribed to the moderately adsorbed H atoms on the Pt surface. Finally the third peak at 925 K is due to H-split-over species [44]. Even though these three peaks are discrete, they are less intense and almost flat as compared to those of the first type of catalyst. The final type of catalyst, $Pt_{72}Ni_{28}$, exhibits a different profile as compared to the other catalysts. In this case, two peaks are observed, a small peak at 604 K and a larger peak at 865 K. An interesting observation of this peak is that it occurs at a lower temperature in comparison to the high temperature peak of Pt_{100}. Hence, it is possible to summarize that Ni may have induced a shift in the latter Pt peak to lower temperature. Li et al. [9] attribute this to the strong interaction between the two metals at lower temperature that consequently improves the H_2-adsorption.

All catalysts investigated desorbed larger amounts of H_2 throughout the analysis as compared to the amounts adsorbed at room temperature (between 1.4×10^{-5} and 4.5×10^{-3} mol $g_{met}{}^{-1}$). However, Ni_{100} and Pt_8Ni_{92} catalysts desorbed the largest quantities of H_2 as tabulated in Table 1. It is important to note that a difference in the amounts desorbed from TPD (4.6×10^{-3} and 6.2×10^{-3} mol $g_{met}{}^{-1}$) and TPR (4.1×10^{-3} and 4.8×10^{-3} mol $g_{met}{}^{-1}$ respectively) studies occurs. This difference may be caused by the different experimental conditions employed in both TP analyses. For H_2-TPD, samples were activated with pure hydrogen for 15 min, hence would incorporate greater quantities of H_2 when compared to the TPR analysis which was conducted in a more diluted environment of 1% H_2. On the other hand it is observed that a lower amount was desorbed by the Pt_{100} catalyst while a moderate amount was incorporated in the $Pt_{21}Ni_{79}$ and $Pt_{72}Ni_{28}$ catalysts. These results correlate well with the TPR profiles shown in Fig. 6.

Further TPD experiments were carried out on the $Pt_{21}Ni_{79}$ catalyst without activation in order to understand the above

Table 1
Average particle size and H_2-TPD studies.

Catalyst denotation (mol ratio)	Total metal content (wt.%)	Total metal content ($\times 10^{-4}$ mol)	Metal content ($\times 10^{-4}$ mol)		Average particle size (nm)[a]	H_{2des} ($\times 10^{-3}$ mol $g_{met}{}^{-1}$)[b]
			Ni	Pt		
Ni_{100}	2.50	4.25	4.25	–	13.6	4.6
Pt_8Ni_{92}	2.98	4.29	3.95	0.34	15.7	6.2
$Pt_{21}Ni_{79}$	2.74	3.12	2.45	0.67	11.6	2.5
$Pt_{21}Ni_{79}$	2.74	3.12	2.45	0.67	–	0.7[c]
$Pt_{72}Ni_{28}$	2.15	1.37	0.38	0.99	9.3	2.4
Pt_{100}	2.82	1.45	–	1.45	6.1	0.3

[a] Calculations based on TEM analysis.
[b] Based on H_2-TPD analysis, after H_2-activation at 473 K then H_2-adsorption at room temperature (see Section 2).
[c] Without H_2-activation at 473 K and H_2-adsorption.

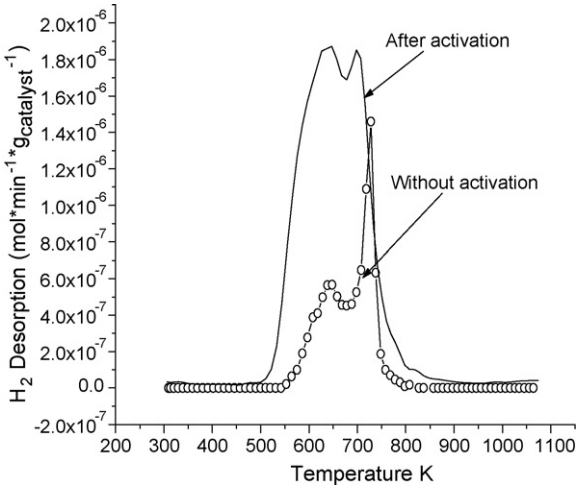

Fig. 8. H_2-TPD profiles of $Pt_{21}Ni_{79}$ without and after activation.

adsorption–desorption phenomenon. Fig. 8 exhibits the profile in comparison with that obtained after activation. It can be seen that two peaks are observed in the profile. These peaks are centred at 600–640 and 727 K. They are similar to that observed for the catalyst after activation as well as that of Pt_8Ni_{92}. This infers that hydrogen adsorbs on similar sites whether it is caused by the reduction process in aqueous media at 353 K or from gaseous hydrogen molecules during the activation process at 473 K. However, additional peaks are observed for the activated catalyst and may be explained as due to the formation of additional Ni° or Pt° sites. Moreover, for $Pt_{72}Ni_{28}$ and Pt_{100} catalysts, absence of peak at 670–750 K strongly indicates that no incorporation of hydrogen during reduction with $NaBH_4$ occurred. Hence, samples containing high amounts of Pt (Pt_{100} and $Pt_{72}Ni_{28}$) show desorption that are contributed by the adsorption during the activation stage. The catalyst without activation, on the other hand, desorbed a lower quantity of H_2 i.e. 0.7×10^{-3} mol g_{met}^{-1}; this is less than 1/3 of the amount desorbed by the activated sample. This desorbed H_2 represents the amount that is adsorbed by the catalyst during the preparation stage (reduction of metal ions). Similar adsorption phenomenon is observed for the Pt_8Ni_{92} and Ni_{100} catalysts. This occurrence has also been observed for supported monometallic nickel catalysts where hydrazine was used as a reducing agent. Hydrazine adsorbs on the support during the preparation stage and then desorbs as nitrogen and hydrogen [45].

Thus the obtained temperature profiles suggest that the formation of alloy nanoparticles modify the sorption properties of the individual metallic components. The presence of one component into the other reduce the adsorption of H_2 onto the catalyst and thus decreases the desorption temperature of hydrogen. Moreover, the bimetallic catalysts seem to indicate the existence of specific sites not observed in the other monometallic catalysts. This occurrence is probably the result of synergistic interaction that occurs between Pt and Ni nanoparticles.

3.2.3. XPS

Fig. 9(a) shows the XPS spectrum of the Pt 4f of the Pt_{100} sample. Two peaks corresponding to the core levels of $4f_{7/2}$ and $4f_{5/2}$ are observed at 71.6 and 74.9 eV respectively. These values correlate to that of the bulk Pt metal which is previously reported at 71.3 and 74.0 eV [46]. Hence, this indicates that the Pt in Pt_{100} is in

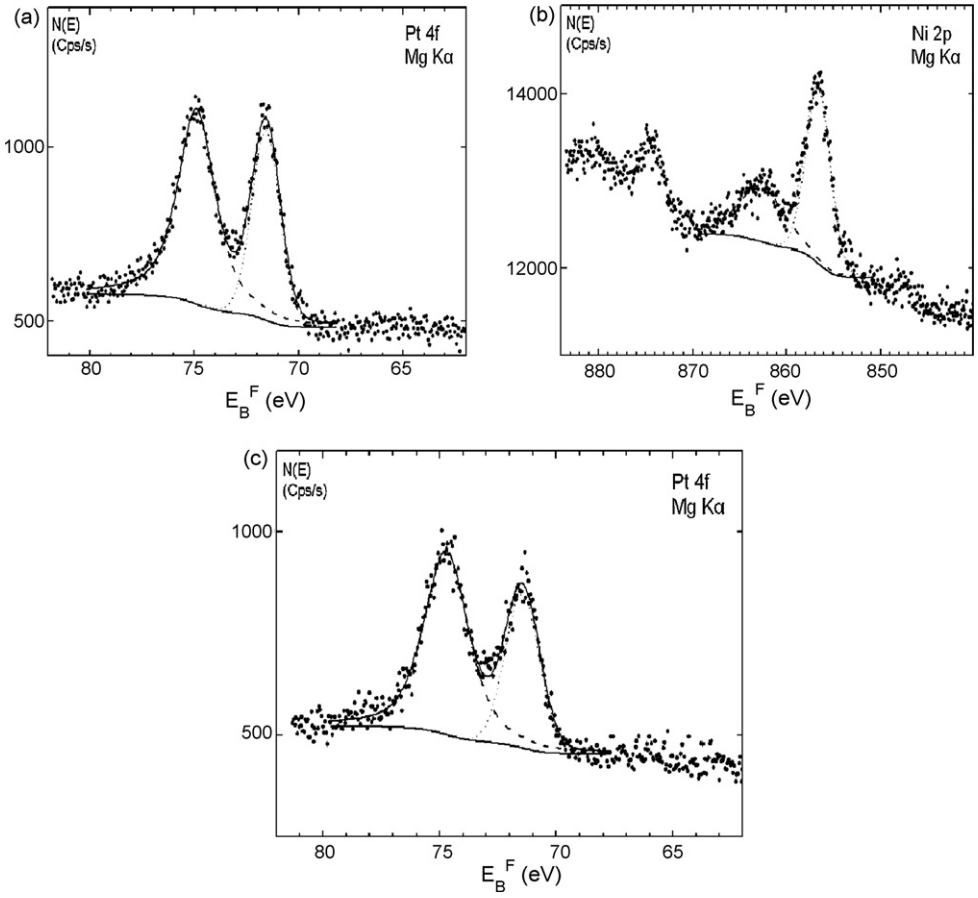

Fig. 9. XPS spectra of (a) Pt 4f of Pt_{100}, (b) Ni 2p of Ni_{100} and (c) Pt 4f of $Pt_{72}Ni_{28}$.

the zerovalent state [46]. The Ni 2p core-shell spectrum of Ni_{100} is shown in Fig. 9(b). The Ni $2p_{3/2}$ exhibits two peaks at 856.6 and 862.9 eV. The peak positioned at 856.6 eV can be attributed to the existence of NiO while the peak at 862.9 is identified as a multielectron excitation satellite peak arising from the high binding energy peak at 856.6 eV [47]. Comparison of these results with that obtained from H_2-TPR studies shows differences in the states in which the Ni exists. H_2-TPR studies indicate that no oxidation occurred contrary to the results obtained via XPS. It is possible that the NiO observed in the XPS profiles may be due to the formation of slight surface oxidation in the samples while the bulk of the metal phase is composed of Ni in the zerovalent state as shown by H_2-TPR studies. In the XPS spectrum of the $Pt_{72}Ni_{28}$ catalyst, similar peaks as to that of the Pt_{100} occurred for the Pt 4f. Here, the $4f_{7/2}$ and $4f_{5/2}$ core levels are positioned at 71.5 and 74.7 eV respectively and are designated to metallic Pt. It is observed that there is a difference of 0.2 eV towards lower binding energies (BE) for the Pt $4f_{7/2}$ core-shell. In addition, no peaks attributed to Ni are observed in the catalyst. These phenomenons are attributed to the occurrence of alloying as well as surface segregation of Pt respectively.

In terms of alloying, the extent in which the peak shifts as a result of alloying is attributed to several factors. Among these factors is the type of interactions that exist between the metals involved and the temperature at which the metals are annealed or activated. Generally, previous works have shown that ionic bonding induces shifts via electron transfer from Ni to Pt [33,46,48]. Zhao et al. showed that a shift of about 0.3 eV to lower BE occurred in the Pt 4f spectra for Pt/Ni nanoparticle alloys supported on multi-walled carbon nanotubes [33]. Park et al. [46] also obtained similar values. However, other researchers have explained that this shift is attributed to variations in the annealing temperature. As an example, Park et al. [49] reported that annealing Pt/Ni electrodes at 300 and 500 °C showed larger XPS peak shifts compared to annealing at 200 °C. In their work, annealing at the latter temperature exhibits a shift of 0.1 eV hence indicates that less alloying occurred compared to when higher temperatures were applied. In this work a shift of 0.2 eV is observed. It is possible that a weak interaction between the Pt and Ni occurred. Metallic bonds which are weaker than ionic bonds may have been formed leading to the small shift. Even so, the low temperature at which the Pt/Ni catalyst was activated may have also contributed to this slight peak shift. This further proves that alloying occurs in the PtNi system prepared in this work.

Surface segregation of the Pt may also occur in the metal phase of the $Pt_{72}Ni_{28}$ catalyst. It is well known that metals with a lower heat of sublimation tend to segregate on the surface of alloys. Considering that the heats of vaporization of Pt and Ni are 509.6 and 370.3 kJ/mol respectively, such thermodynamic explanation is not applicable in the case of Pt/Ni alloys [46]. Hence, other theories have been put forward to explain this occurrence. One of the most widely accepted theories is based on the electronic structure of the metals. Hugosson et al. [50] described that the size of atoms play a significant role in the surface segregation in alloys. Larger atoms tend to have a shorter bonding distance with their nearest neighbours compared to smaller atoms. Such structures exhibit lower surface energy. Thus, stable alloys are formed by forcing the larger atoms to the surface where the coordination number is even smaller. In this work, the larger size of the Pt atoms compared to Ni, leads to segregation of the Pt on the Pt/Ni alloy surface. The total Ni content, which is 27.5 at%, is retained in the bulk of the Pt/Ni alloy making it undetectable via XPS. Similar finding has been reported elsewhere [30].

3.3. Effect of borohydride reduction

The possible formation of NiB or PtB is also another important aspect that requires consideration as the work described employs $NaBH_4$ as the reducing agent. Several authors have reported the formation of NiB via the reduction of Ni salts using KBH_4 [26,51,52]. We presume that PtB alloying does not occur due to the stable nature of Pt. Several studies on the incorporation of Pt and B on various supports have shown that only interaction between the support and B occurred [53,54]. The possible amorphous nature of NiB prevents the determination of this compound via XRD, if it occurs. This gives rise to the possibility of NiB existing in the catalysts however the extent in which it is present is unknown. XPS investigations of the Ni $2p_{3/2}$ spectrum show that no peaks signifying the availability of NiB arise at approximately ~853 eV. Even so, AAS analysis reveals that only 0.27 wt% of boron exists in the Ni_{100} catalysts. This indicates that the formation of NiB, if any, is limited. Interestingly the bimetallic catalysts and Pt_{100} exhibit the presence of even less boron content. The Pt_{100}, $Pt_{72}Ni_{28}$, $Pt_{21}Ni_{79}$ and Pt_8Ni_{92} contain 0.01–0.15 wt% of boron. Here, boron content decreases with Ni content. It is well known that unlike Pt, Ni easily forms NiB via the donation of electrons from B to metallic Ni making B electron deficient and Ni electron rich [26]. Hence, this may explain the higher availability of boron in catalysts with high Ni content. These alloys have highly unsaturated coordinative sites that promotes adsorption and surface reactions [55]. Therefore this elucidates the adsorption of H_2 by catalysts with high Ni content upon reduction of the metal ions with $NaBH_4$ as observed via H_2-TPD analysis.

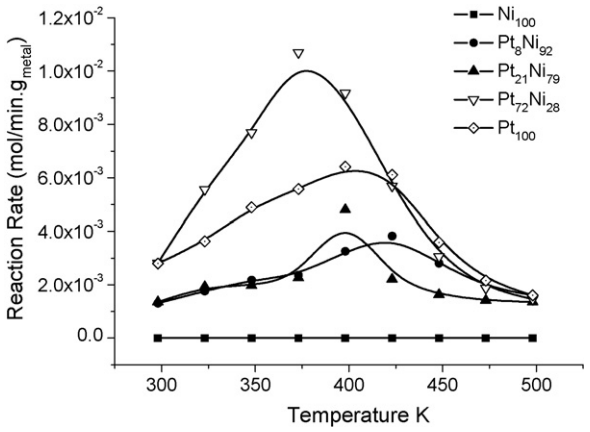

Fig. 10. Profiles of the reaction rate of hydrogenation of benzene to cyclohexane for various Pt/Ni catalysts supported on crystalline silica relative to the reaction temperature.

3.4. Hydrogenation of benzene

The reaction rates of the various Pt/Ni catalysts as a function of temperature were investigated for the hydrogenation of benzene to cyclohexane and are illustrated in Fig. 10. Analysis of the support mixed with $NaBH_4$ (not shown in Fig. 10) exhibited no activity at all. Pt/Ni catalysts on the other hand showed an increase in reaction rates and a shift towards lower temperatures with increasing Pt content. The Ni_{100} catalyst showed no reaction rates, similar to that of the support mixed with $NaBH_4$ in the temperature range studied. However, incorporation of Pt in the catalysts resulted in drastic increases in the reactions rates. Both Pt_8Ni_{92} and $Pt_{21}Ni_{79}$ exhibited reaction rates of approximately 3.5×10^{-3} mol min $g_{met}{}^{-1}$ at 420 and 397 K respectively. Further increase of the Pt content in the catalyst $Pt_{72}Ni_{28}$ demonstrated an even higher reaction rate of 10.7×10^{-3} mol min $g_{met}{}^{-1}$ at 368 K. Interestingly this is 4.4×10^{-3} mol min $g_{met}{}^{-1}$ higher than that of the Pt_{100} catalyst which exhibits maximum reaction rates at 400 K.

High reaction rates are always observed for aromatic hydrogenation over group VIII metal catalysts [56]. Hence, bimetallic catalysts

containing a metal from this group have frequently shown high reaction rates. Research on the Pt/Ni systems suggested that the occurrence of synergistic effects between Ni and Pt upon alloying occur [33,34,57]. This influences the metal's electronic structure and indirectly the chemisorption properties of the molecules/atoms on the metals involved hence changes the reaction rates. Numerous factors can change the electronic structure as a result of alloying. Among these are the difference in Pt–Pt bond distance, number of Pt nearest neighbours as well as electron density of the Pt d orbital [3,34].

In this study, the high reaction rate exhibited by the Pt_8Ni_{92} and $Pt_{21}Ni_{79}$ catalysts as compared to Ni_{100} may be explained as due to the presence of Pt in the bimetallic catalysts. However, the enhanced reaction rate of the $Pt_{72}Ni_{28}$ when compared to the Pt_{100} catalysts can be attributed to several factors. Comparison of the average particle sizes of Pt_{100} and $Pt_{72}Ni_{28}$ indicates that Pt_{100} particles are smaller however reactivity of the $Pt_{72}Ni_{28}$ is much higher. This signifies that the morphology of the metal particles did not affect the reactivity and emphasizes that the reactivity may be attributed to alloying between the Pt and Ni metals. This was shown previously via line analysis and XPS results. Surface segregation of Pt which is more active than Ni atoms, seen in the XPS studies could have also played a role in promoting the reactivity of this catalyst. In this system, contribution of NiB, if any, to the reaction rate is minimal considering Ni_{100} which contains the highest B content exhibits inactivity towards the hydrogenation of benzene to cyclohexane.

4. Conclusion

The present study shows that the catalysts preparation method employed facilitates the formation of totally reduced bimetallic metal particles. TEM analysis reveals that the metal phase in the Pt_{100}, Ni_{100} and $Pt_{72}Ni_{28}$ catalysts exist as fractal morphologies. Fractal dimension of the catalysts indicates that in contrast to Ni_{100}, the Pt_{100} and bimetallic $Pt_{72}Ni_{28}$ are composed of active phases suitable for catalytic reactions. Enhanced activity is seen for all bimetallic catalysts when compared to Ni_{100}. Even so, the best catalytic activity is seen for the $Pt_{72}Ni_{28}$. Results indicate that alloying and Pt segregation on the surface of the alloys are factors that lead to the improved conversion of benzene.

Acknowledgements

The authors would like to acknowledge the financial support from Communauté Urbaine du Grand Nancy, University Sains Malaysia, Université Henri Poincare, the French and Malaysian governments for the Co-tutelle and ASTS scholarship for N.H.H. Abu Bakar. They also thank J. Ghanbaja (Service commun de microscopies électroniques, UHP) for the Electron Microscope recordings.

References

[1] J. Ning, J. Xu, J. Liu, F. Lu, Catal. Lett. 109 (2006) 175–180.
[2] M. Neergat, A.K. Shukla, K.S. Gandhi, J. Appl. Electrochem. 31 (2001) 373–378.
[3] L. Xiong, A.M. Kannan, A. Manthiram, Electrochem. Commun. 4 (2002) 898–903.
[4] J.R.C. Salgado, E. Antolini, E.R. Gonzalez, J. Power Sources 141 (2005) 13–18.
[5] Z.B. Wang, G.P. Yin, P.F. Shi, J. Alloys Compd. 420 (2006) 126–132.
[6] E. Blosma, J.A. Martens, P.A. Jacobs, J. Catal. 165 (1997) 241–248.
[7] E. Antolini, Mater. Chem. Phys. 78 (2003) 563–573.
[8] M.A. Gracia-Contreras, S.M. Fernandez-Valverdi, J.R. Vargas-Gracia, J. Alloys Compd. 434–435 (2007) 522–524.
[9] Y. Li, G.H. Lai, R.-X. Zhou, Appl. Surf. Sci. 253 (2007) 4978–4984.
[10] E. Antolini, J.R.C. Salgado, R.M. da Silva, E.R. Gonzalez, Mater. Chem. Phys. 101 (2007) 395–403.
[11] Z. Xiong, Z. Mi, X. Zhang, Catal. Commun. 8 (2007) 571–575.
[12] Y. He, M. Qiao, H. Hu, J.-F. Deng, K. Fan, Appl. Catal. A: Gen. 228 (2002) 29–37.
[13] K. Torigoe, Y. Nakajima, K. Esumi, J. Phys. Chem. 97 (1993) 8304–8309.
[14] M. Mandal, S. Kundu, S.K. Ghosh, T.K. Sau, S.M. Yusuf, T. Pal, J. Colloid Interface Sci. 265 (2003) 23–28.
[15] T.C. Deivaraj, W. Chen, J.Y. Lee, J. Mater. Chem. 13 (2003) 2555–2560.
[16] A.-G. Boudjahem, M. Pietrowski, S. Monteverdi, M. Mercy, M.M. Bettahar, J. Mater. Sci. 41 (2006) 2025–2030.
[17] M.M. Telkar, J.M. Nadgeri, C.V. Rode, R.V. Chaudhari, Appl. Catal. A: Gen. 295 (2005) 23–30.
[18] Y. Liang, H. Zhang, B. Yi, Z. Zhang, Z. Tan, Carbon 43 (2005) 3144–3152.
[19] S. Zhou, B. Varghese, B. Eichhorn, G. Jackson, K. McIlwrath, Angew. Chem. 117 (2005) 4615–4619.
[20] S. Sun, C.B. Murray, D. Weller, L. Folks, A. Moser, Science 287 (2000) 1989–1992.
[21] J. Luo, M.M. Maye, V. Petkov, N.N. Kariuki, L. Wang, P. Njoki, D. Mott, Y. Li, C.-J. Zhong, Chem. Mater. 17 (2005) 3086–3091.
[22] G. Mattei, Nucl. Instrum. Methods B 191 (2002) 323–332.
[23] H.M. Chen, H.-C. Peng, R.S. Liu, S.F. Hu, L.-Y. Jang, Chem. Phys. Lett. 420 (2006) 484–488.
[24] R. Wojcieszak, S. Monteverdi, M. Mercy, I. Nowak, M. Ziolek, M.M. Bettahar, Appl. Catal. A: Gen. 268 (2004) 241–253.
[25] R. Wojcieszak, S. Monteverdi, J. Ghanbaja, M.M. Bettahar, J. Colloid Interface Sci. 317 (2008) 166–174.
[26] H. Li, Hexing Li, J.F. Deng, Catal. Today 74 (2002) 53–63.
[27] J.Z. Liang, Compos. Part A: Appl. Sci. Manuf. 38 (2007) 1502–1506.
[28] A. Borodzinski, M. Bonarowska, Langmuir 13 (1997) 5613–5620.
[29] Y. Koltypin, G. Katabi, X. Cao, R. Prozorov, A. Gedanken, J. Non-Cryst. Solids 201 (1996) 159–162.
[30] S.Y. Choi, Y.S. Kwon, S.C. Hong, J.I. Lee, R.Q. Wu, J. Magn. Magn. Mater. 226–230 (2001) 1662–1663.
[31] L. Hammer, M. Kottcke, M. Taubmann, S. Meyer, C. Rath, K. Heinz, Surf. Sci. 431 (1999) 220–231.
[32] P. Deurinck, C. Creemers, Surf. Sci. 441 (1999) 493–506.
[33] Y. Zhao, E. Yifeng, L. Fan, Y. Qiu, S. Yang, Electrochim. Acta 52 (2007) 5873–5878.
[34] H. Yang, W. Vogel, C. Lamy, N. Alonso-Vante, J. Phys. Chem. B 108 (2004) 11024–11034.
[35] X. Zheng, L. Zhu, X. Wang, A. Yan, Y. Xie, J. Cryst. Growth 260 (2004) 255.
[36] Z.W. Chen, J.K.L. Lai, C.H. Shek, H.D. Chen, Appl. Surf. Sci. 250 (2005) 3–8.
[37] E. Nouri, A. Dolati, Mater. Res. Bull. 42 (2007) 1769–1776.
[38] T. Pajkossy, L. Nyikos, Electrochim. Acta 34 (1989) 171–179.
[39] J. Li, N.J. Coville, Appl. Catal. A: Gen. 181 (1999) 201–208.
[40] L. Chen, Y. Lua, Q. Hong, J. Lin, F.M. Dautzenberg, Appl. Catal. A: Gen. 292 (2005) 295–304.
[41] U.A. Paulus, A. Wokaun, G.G. Scherer, T.J. Schmidt, V. Stamenkovic, V. Radmilovic, N.M. Markovic, P.N. Ross, J. Phys. Chem. B 106 (2002) 4181–4191.
[42] P. Sivakumar, R. Ishak, V. Tricoli, Electrochim. Acta 50 (2005) 3312–3319.
[43] S. Chettibi, R. Wojcieszak, E.H. Boudjennad, J. Belloni, M.M. Bettahar, N. Keghouche, Catal. Today 113 (2006) 157–165.
[44] W. Curtis Conner Jr., J.L. Falconer, Chem. Rev. 95 (1995) 759–788.
[45] A. Jasik, R. Wojcieszak, S. Monteverdi, M. Ziolek, M.M. Bettahar, J. Mol. Catal. A: Chem. 242 (2005) 81–90.
[46] K.-W. Park, J.H. Choi, B.K. Kwoon, S.-A. Lee, Y.-E. Sung, H.-Y. Ha, S.-A. Hong, H. Kim, A. Wieckowski, J. Phys. Chem. B 106 (2002) 1869–1877.
[47] F. Liu, J.Y. Lee, W. Zhou, J. Phys. Chem. B 108 (2004) 17959–17963.
[48] F. Liu, J.Y. Lee, W.J. Zhou, Small 2 (1) (2006) 121–128.
[49] K.-W. Park, J.-H. Choi, Y.-E. Sung, J. Phys. Chem. B 107 (2003) 5851–5856.
[50] H.W. Hugosson, O. Eriksson, U. Jansson, I.A. Abrikosov, Surf. Sci. 585 (2005) 101–107.
[51] Y. Lu, J. Li, J. Lin, Catal. Lett. 76 (2001) 167–175.
[52] Y. Feng, Y. Li, H. Yuan, J. Alloys Compd. 468 (2009) 575–580.
[53] M. Hatano, H. Kinoshita, Appl. Surf. Sci. 121–122 (1997) 278–285.
[54] D. Hullmann, G. Wendt, U. Singliar, G. Ziegenbalg, Appl. Catal. A: Gen. 225 (2002) 261–270.
[55] R. Zhang, F. Li, N. Zhang, Q. Shi, Appl. Catal. A: Gen. 239 (2003) 17–23.
[56] M.A. Keane, J. Catal. 166 (1997) 347–355.
[57] J.F. Drillet, A. Ea, J. Freidemann, R. Kotz, B. Schnyder, V.M. Schmidt, Electrochim. Acta 47 (2002) 1983–1988.